Combination of Ribociclib with BET-Bromodomain and PI3K/mTOR Inhibitors for Medulloblastoma Treatment *In Vitro* and *In Vivo*

Barbara Jonchere[1], Justin Williams[1], Frederique Zindy[1], Jingjing Liu[2], Sarah Robinson[1], Dana M. Farmer[1], Jaeki Min[3], Lei Yang[3], Jennifer L. Stripay[1], Yingzhe Wang[4], Burgess B. Freeman III[4], Jiyang Yu[2], Anang A. Shelat[3], Zoran Rankovic[3], and Martine F. Roussel[1]

ABSTRACT

Despite improvement in the treatment of medulloblastoma over the last years, numerous patients with MYC- and MYCN-driven tumors still fail current therapies. Medulloblastomas have an intact retinoblastoma protein RB, suggesting that CDK4/6 inhibition might represent a therapeutic strategy for which drug combination remains understudied. We conducted high-throughput drug combination screens in a Group3 (G3) medulloblastoma line using the CDK4/6 inhibitor (CDK4/6i) ribociclib at IC_{20}, referred to as an anchor, and 87 oncology drugs approved by FDA or in clinical trials. Bromodomain and extra terminal (BET) and PI3K/mTOR inhibitors potentiated ribociclib inhibition of proliferation in an established cell line and freshly dissociated tumor cells from intracranial xenografts of G3 and Sonic hedgehog (SHH) medulloblastomas *in vitro*. A reverse combination screen using the BET inhibitor JQ1 as anchor, revealed CDK4/6i as the most potentiating drugs. *In vivo*, ribociclib showed single-agent activity in medulloblastoma models whereas JQ1 failed to show efficacy due to high clearance and insufficient free brain concentration. Despite *in vitro* synergy, combination of ribociclib with the PI3K/mTOR inhibitor paxalisib did not significantly improve the survival of G3 and SHH medulloblastoma-bearing mice compared with ribociclib alone. Molecular analysis of ribociclib and paxalisib-treated tumors revealed that E2F targets and PI3K/AKT/MTORC1 signaling genes were depleted, as expected. Importantly, in one untreated G3MB model HD-MB03, the PI3K/AKT/MTORC1 gene set was enriched *in vitro* compared with *in vivo* suggesting that the pathway displayed increased activity *in vitro*. Our data illustrate the difficulty in translating *in vitro* findings *in vivo*.

See related article in Mol Cancer Ther (2022) 21(8):1306–1317.

Introduction

Medulloblastoma is the most common malignant pediatric brain tumor with a median age of 7 years at diagnosis (1). Among the four subgroups, Group 3 (G3MB) with *MYC* overexpression by amplification or not and Sonic hedgehog (SHHMB) with *MYCN* amplification and *TP53* mutations have the poorest outcome (1, 2). In all cases, limited therapeutic options exist when tumors recur. Extensive molecular analysis from hundreds of medulloblastoma primary patient samples revealed that the retinoblastoma signaling pathway is often compromised, including amplification of *CDK4*, *CDK6* or *CCND2* whereas retinoblastoma itself remains intact (3) making CDK4/6 inhibitors (CDK4/6i) an attractive therapeutic strategy for medulloblastoma (4).

Three FDA-approved CDK4/6i, palbociclib (Pfizer), abemaciclib (Eli Lilly), and ribociclib (Novartis) are in clinical trials for multiple cancers. Although monotherapy induces disease stabilization in a small percentage of patients, CDK4/6i are more active in combination (5). All three clinically used CDK4/6i were shown to efficiently treat HR^+ $HER2^-$ advanced breast cancer in combination with endocrine therapy (6), and are being evaluated with other drug partners.

Ribociclib was previously shown to cross the blood–brain barrier (7) and is currently evaluated in combination with gemcitabine, trametinib or sonidegib in a clinical trial at SJCRH for children with recurrent medulloblastoma (SJDAWN, NCT03434262). To identify additional compounds that synergize with ribociclib, we devised a combination drug screen in which one drug (referred to as anchor) used at a single concentration of 20% of the IC_{20} value, was tested with 87 oncology drugs in dose–response. We used medulloblastoma tumor cells from human G3MB established cell lines or from freshly dissociated tumor cells harvested from mice harboring intracranial patient-derived G3MB and SHH medulloblastoma xenografts (PDX). Anchor drugs were either ribociclib or the bromodomain and extra terminal (BET) inhibitor (BETi) JQ1 (8), used for validation. BETi and PI3K/mTOR inhibitors synergized with ribociclib in *vitro* and were evaluated in preclinical models of G3MB and SHHMB.

Materials and Methods

Human G3MB cell lines and PDXs

Human G3MB established cell lines, HD-MB03 and MB002 were generously provided by Drs. Till Milde and Jae-Youn Cho, respectively (9, 10). PDXs SJMBG3–12–5950, SJMBG3–16–08522, SJMBSHH-13–5634, and SJMBSHH-14–7196 were previously described (11). *In vivo* studies were performed in female Crl:CD1-Foxn1nu (CD-1

[1]Department of Tumor Cell Biology, St. Jude Children's Research Hospital, Memphis, Tennessee. [2]Department of Tumor Cell Biology Computational Biology, St. Jude Children's Research Hospital, Memphis, Tennessee. [3]Department of Tumor Cell Biology Chemical Biology, St. Jude Children's Research Hospital, Memphis, Tennessee. [4]Department of Tumor Cell Biology Preclinical PK Shared Resource, St. Jude Children's Research Hospital, Memphis, Tennessee.

Current address for J. Min: Amgen Inc., Thousand Oaks, CA; and current address for J.L. Stripay: Communication and Science/Medical Content Outreach, St. Jude Children's Research Hospital, Memphis, TN.

Corresponding Author: Martine F. Roussel, St. Jude Children's Research Hospital, MS#350, 262, Danny Thomas Place, Memphis, TN 38105. Phone: 901-595-3481; Fax: 901-595-2384; E-mail: martine.roussel@stjude.org

Mol Cancer Ther 2023;22:37–51

doi: 10.1158/1535-7163.MCT-21-0896

This open access article is distributed under the Creative Commons Attribution-NonCommercial-NoDerivatives 4.0 International (CC BY-NC-ND 4.0) license.

©2022 The Authors; Published by the American Association for Cancer Research

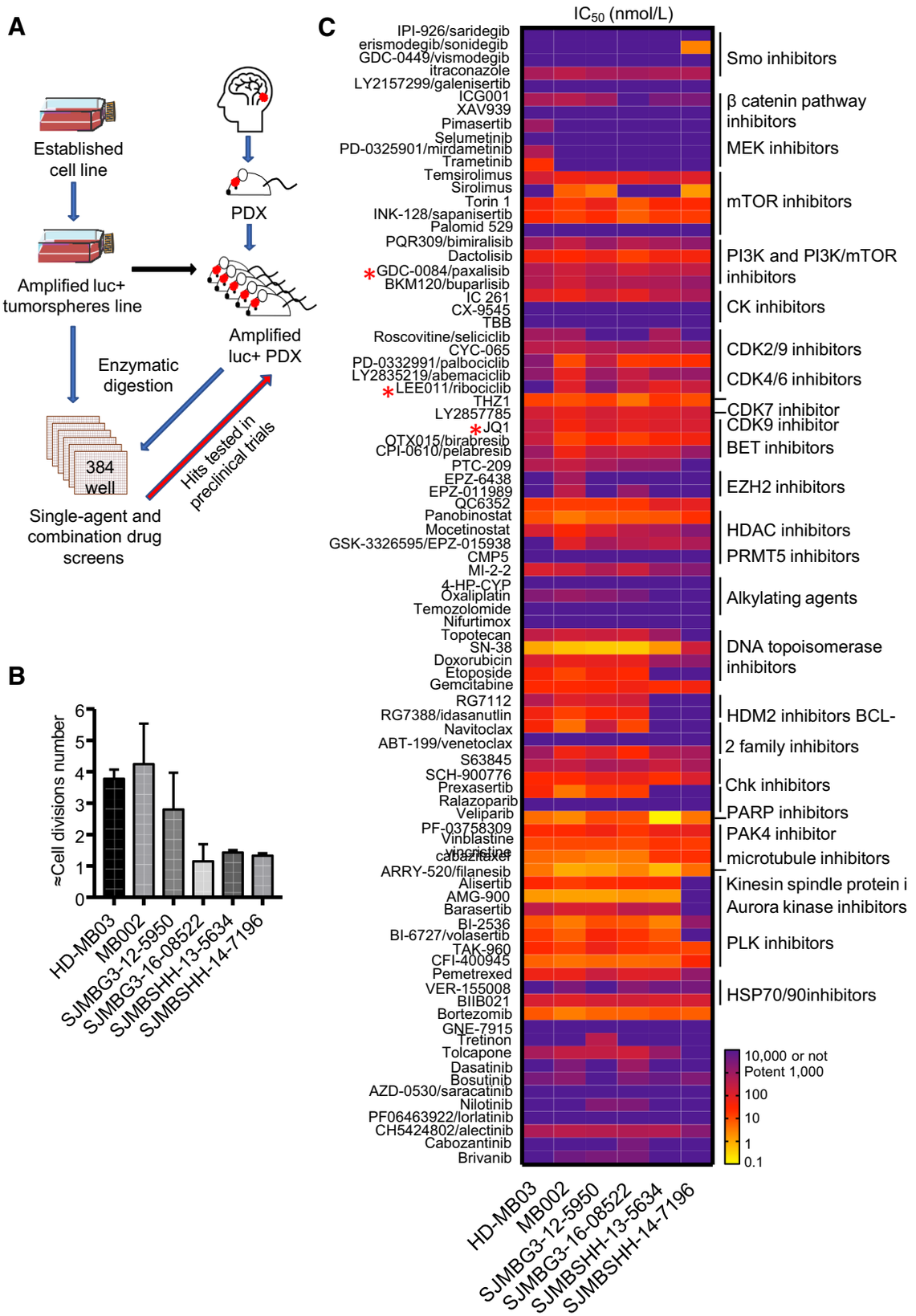
A
Established cell line
Amplified luc+ tumorspheres line
Enzymatic digestion
384 well
Single-agent and combination drug screens
Hits tested in preclinical trials
PDX
Amplified luc+ PDX
B
≈Cell divisions number
0
1
2
3
4
5
6
HD-MB03
MB002
SJMBG3-12-5950
SJMBG3-16-08522
SJMBSHH-13-5634
SJMBSHH-14-7196
C
IC50 (nmol/L)
IPI-926/saridegib
erismodegib/sonidegib
GDC-0449/vismodegib
itraconazole
LY2157299/galenisertib
ICG001
XAV939
Pimasertib
Selumetinib
PD-0325901/mirdametinib
Trametinib
Temsirolimus
Sirolimus
Torin 1
INK-128/sapanisertib
Palomid 529
PQR309/bimiralisib
Dactolisib
*GDC-0084/paxalisib
BKM120/buparlisib
IC 261
CX-9545
TBB
Roscovitine/seliciclib
CYC-065
PD-0332991/palbociclib
LY2835219/abemaciclib
*LEE011/ribociclib
THZ1
LY2857785
*JQ1
OTX015/birabresib
CPI-0610/pelabresib
PTC-209
EPZ-6438
EPZ-011989
QC6352
Panobinostat
Mocetinostat
GSK-3326595/EPZ-015938
CMP5
MI-2-2
4-HP-CYP
Oxaliplatin
Temozolomide
Nifurtimox
Topotecan
SN-38
Doxorubicin
Etoposide
Gemcitabine
RG7112
RG7388/idasanutlin
Navitoclax
ABT-199/venetoclax
S63845
SCH-900776
Prexasertib
Ralazoparib
Veliparib
PF-03758309
Vinblastine
vincristine
cabazitaxel
ARRY-520/filanesib
Alisertib
AMG-900
Barasertib
BI-2536
BI-6727/volasertib
TAK-960
CFI-400945
Pemetrexed
VER-155008
BIIB021
Bortezomib
GNE-7915
Tretinon
Tolcapone
Dasatinib
Bosutinib
AZD-0530/saracatinib
Nilotinib
PF06463922/lorlatinib
CH5424802/alectinib
Cabozantinib
Brivanib
Smo inhibitors
β catenin pathway inhibitors
MEK inhibitors
mTOR inhibitors
PI3K and PI3K/mTOR inhibitors
CK inhibitors
CDK2/9 inhibitors
CDK4/6 inhibitors
CDK7 inhibitor
CDK9 inhibitor
BET inhibitors
EZH2 inhibitors
HDAC inhibitors
PRMT5 inhibitors
Alkylating agents
DNA topoisomerase inhibitors
HDM2 inhibitors BCL-
2 family inhibitors
Chk inhibitors
PARP inhibitors
PAK4 inhibitor
microtubule inhibitors
Kinesin spindle protein i
Aurora kinase inhibitors
PLK inhibitors
HSP70/90inhibitors
10,000 or not Potent 1,000
100
10
1
0.1
HD-MB03
MB002
SJMBG3-12-5950
SJMBG3-16-08522
SJMBSHH-13-5634
SJMBSHH-14-7196

nude) mice (Charles River Laboratories). Tumors were labeled with firefly luciferase for *in vivo* bioluminescence imaging (BLI), as previously described (12). Marked tumor cells were amplified, banked, and routinely tested by DNA fingerprinting to ensure tumor identity. Mice were housed in an AAALAC-accredited facility. Studies were approved by the Animal Care and Use Committee and performed in accordance with best practices outlined by the NIH Office of Laboratory Animal Welfare.

High-throughput drug screens

Tumor cells were seeded in 384-well plates. For a detailed method of cell culture condition, tumor dissociation and cell density optimization, see Supplementary Material. 2 to 24 hours after seeding, 87 compounds in 10 concentrations dose–response were pin-transferred to plates using the Biomek FX Laboratory Automation Workstation (Beckman Coulter, Inc.). 0.08% DMSO and 1.6 μmol/L staurosporine were used as negative and positive controls, respectively. 7 days after treatment, cell proliferation was measured using CellTiter-Glo reagent (Promega, G7375). For the anchor-based combination screen, cells were drugged with a single dose IC_{20} value of the anchor, 5 μmol/L ribociclib or 132 nmol/L JQ1, or 0.08% DMSO against up to 87 compounds in dose–response. IC_{50} values of the 87 compounds, with or without the anchor, were computed using RISE (Robust Investigation of Screening Experiments), an in-house program. To evaluate synergy, cells were drugged with ribociclib and the drug partner (JQ1 or the PI3K/mTORi paxalisib) in dose–response and data were analyzed using Bivariate Response to Additive Interacting Doses (BRAID) response surface model (13). For more details of the high-throughput screen (HTS), washout experiment, cell cycle, Annexin V analysis and immunoblotting methods, see Supplementary Material.

Brain tissue binding (equilibrium dialysis)

Brain tissue binding of a compound and free drug concentration were determined using rapid equilibrium dialysis in which the aqueous component of the brain homogenate containing the free compound diffuses through the dialysis membrane (MWCO 12k). For more details and for plasma tissue binding method, see Supplementary Material.

In vivo mouse brain exposure assessment

7–11-week-old female Crl:CD1 (ICR) mice (Charles River Laboratories) were used for *in vivo* pharmacokinetic (PK) profiling. Whereas there can be a significant difference in drug metabolism between the sexes in rodents (14, 15), limiting the analysis to one sex minimizes inter-mouse variability in drug exposure. Blood and brain samples were harvested at 0.083, 1, and 4 hours after dose (three animals at each time point) and were analyzed for drug concentration by LC-MS/MS. For a detailed method, see Supplementary Material.

JQ1 PK study

A single dose of JQ1 was administered to non–tumor-bearing mice intraperitoneally at 50 mg/kg. Perfused brain tissues were harvested at 0.5, 1, 2, 4, 8, and 24 hours after dose (three animals at each time point) and drug concentrations were quantified as described previously in Supplementary Material. Brain tissue binding data were used to compute free unbound concentrations.

MTD evaluation

To determine which dose of paxalisib was tolerated when combined with 100 mg/kg of ribociclib, three groups of non-tumor bearing mice (3 mice each) were dosed daily with ribociclib combined with 5, 10 or 15 mg/kg of paxalisib for 3 weeks. Three control groups received vehicle, ribociclib at 100 mg/kg, or paxalisib at 15 mg/kg daily for 3 weeks. Toxicity was evaluated as described below.

Preclinical trials

Luciferase-positive HD-MB03 and MB002 lines ($\sim 1\times10^5$ cells/mouse) or PDX tumor cells SJMBG3–12–5950 and SJMBSHH-13–5634 ($\sim 1\times10^6$ cells/mouse) were resuspended in 5 μL Matrigel (BD Biosciences, 356234) and stereotactically implanted in the cortices of 7–11-week-old female CD-1 nude mice. Tumor growth was assessed twice weekly by BLI, as previously described (12). Treatment was initiated when BLI reached approximately 5×10^5 photons/second (p/s) for G3MB lines and approximately 1×10^6 p/s for PDXs. Mice were randomized into treatment arms and dosed continuously with vehicle, ribociclib, JQ1, paxalisib, the combination of ribociclib and JQ1 or ribociclib and paxalisib until animals became moribund. Drug formulation, administration, and doses are described previously in the Supplementary Material. Mice that reached endpoint were euthanized and tumors were harvested and snap-frozen for molecular analysis. Mice were excluded from the analysis if they died or required humane euthanasia without tumor burden. Mice experiencing severe body weight loss unrelated to tumor burden, indicative of toxicity, were included in the analysis.

Toxicity measurement

Toxicity was monitored by measuring body weights daily and by performing blood work at baseline and every 2 weeks or after 3 weeks of treatment. Complete blood counts and diagnostic chemistry panels were performed, as previously described (12).

Molecular analysis

RNA from snap-frozen tumors was extracted using TRizol (Ambion, 15596026). After QC and library preparation, the library was sequenced using Illumina NovaSeq 6000. For RNA sequencing analysis, including gene set enrichment, differentially expressed genes (DEG) and gene set variation analyses see Supplementary Material.

Statistical analysis

Statistical significance between treatment groups for overall survival was determined by the log-rank test (Mantel–Cox) adjusted for multiple comparisons (Holm–Sidak method). Other statistical analyses were performed using the Mann–Whitney test. GraphPad Prism version 7.0a for Mac (GraphPad Software, www.graphpad.com) was used for all analyses. Results were considered significant if P or

Figure 1.

Drug screens using tumorspheres and fresh tumor cells from G3MB and SHHMB PDX. **A,** Drug-screening strategy using tumorspheres (HD-MB03) and fresh tumor cells dissociated from intracranial PDXs (MB002, SJMBG3–12–5950, SJMBG3–16–08522, SJMBSHH-13–5634, and SJMBSHH-14–7196). Synergistic and additive combinations tested in preclinical trials using G3MB and SHHMB PDX-bearing mice. **B,** Approximation of the number of cell divisions of untreated cells during 7 days of incubation in 384-well plates. CellTiter Glo reagent used on untreated cells on days 0 and 7. RLU fold change computed and $\log_2$ transformed. 1,000 cells per well density for all models ($n = 3$–7). **C,** The IC_{50} heatmap of the 87 drugs assayed as single agent in the different cell models after 7 days of treatment ($n = 3$ and technical duplicate or triplicate for each). * Compounds used *in vivo* identified with a red star. Raw data are presented in Supplementary Table S1.

adjusted $P \leq 0.05$ (*, $P < 0.05$; **, $P < 0.01$; ***, $P < 0.001$). Data were graphed as the mean values ± SD unless stated otherwise.

Data availability

RNA sequencing data generated in this study have been deposited to the St. Jude Cloud except for HDMB03 cells deposited in the EGA under session EGAS00001006286

Results

In vitro drug screens

Although several human G3MB cell lines (16) grow *in vitro* as tumorspheres, we were unable to establish cell lines from intracranial PDXs (11). We developed a protocol that allowed freshly dissociated cells from tumors harvested from the brain of mice harboring PDXs to grow for 7 days in culture in 384-well plate (**Fig. 1A**) with 2–4 doubling times (**Fig. 1B**) and with high assay quality, z prime > 0.5 (Supplementary Material, Supplementary Fig. S1). Tumor cells were screened against 87 selected compounds in a 10 concentrations dose–response (10 μmol/L to 0.14 nmol/L). Many compounds inhibited proliferation (**Fig. 1C**; Supplementary Table S1). SN38 (DNA topoisomerase I inhibitor), PF-03758309 (PAK4 inhibitor), filanesib (kinesin spindle protein inhibitor), and AMG900 (pan-Aurora kinases inhibitor) were the most potent with the IC_{50} value in the picomolar to low nanomolar range. mTOR, PI3K, CDK, BET, and PLK inhibitors inhibited the proliferation of all lines tested. Ribociclib was potent *in vitro* in most of the six medulloblastoma models that included HD-MB03 cells and five freshly dissociated cells from intracranial medulloblastoma PDXs. The MB002 model was the most sensitive to ribociclib.

In vitro drug combination screens

To identify compounds that potentiate ribociclib activity, we designed a combination screen using HD-MB03 cells in which ribociclib, referred to as the anchor drug, was used at one concentration ($IC_{20} = 5$μmol/L), and screened against the panel of 87 compounds in dose–response (10 μmol/L to 0.14 nmol/L). Cells were treated once with ribociclib plus drug partners. Growth inhibition was measured 7 days later. Compounds showed a wide range of potency as single agents (**Fig. 1C**; Supplementary Table S1; **Fig. 2A**). When comparing IC_{50} values of the 87 compounds with or without ribociclib, 11 compounds reached the 3-fold improvement threshold as potential synergistic combinations (**Fig. 2A** and **B**). Among the top 11 drugs, three BETi, birabresib (OTX-015), pelabresib (CPI-0610), and JQ1 synergized with ribociclib, birabresib, and pelabresib reaching 10-fold IC_{50} improvement (**Fig. 2B**; Supplementary Fig. S2A; Supplementary Table S1). Other top compounds included three MEKi (mirdametinib (PD-0325901), pimasertib and trametinib) and three PI3K/mTORi [sapanisertib (INK128), buparlisib (BKM120) and bimiralisib (PQR309); **Fig. 2B**; Supplementary Fig. S2B and S2C; Supplementary Table S1].

To validate the potentiation between ribociclib and BETi revealed by the ribociclib combination screen (**Fig. 2A** and **B**), we performed a combination screen in HD-MB03 cells using JQ1 as the anchor drug (IC_{20} = 132 nmol/L). In this reverse combination screen, 59 compounds were used in dose–response (**Fig. 2C**), 90% of them included in the original compounds list of 87 (Supplementary Table S2). Remarkably, the top candidate drugs that synergized with JQ1 included the three CDK4/6i exceeding 3-fold improvement of the IC_{50} value threshold with 30.5-fold for palbociclib, 12.8-fold for abemaciclib, and 7.8-fold for ribociclib (**Fig. 2D**; Supplementary Fig. S2D; Supplementary Table S1). Similar to the data from the combination screen with ribociclib as the anchor drug, the other top candidate drugs included MEKi and PI3Ki (**Fig. 2D**; Supplementary Table S1).

When tested as single agents, CDK4/6i, BETi, and PI3K/mTORi inhibited tumor cell proliferation of the HD-MB03 line, three G3MB PDXs, and two SHH medulloblastoma PDXs (Supplementary Fig. S3A–S3C). In contrast, MEKi were less effective except in HD-MB03 (Supplementary Fig. S3D).

Ribociclib and the BETi JQ1 synergize to inhibit G3MB proliferation *in vitro*

We combined ribociclib and JQ1 each in dose–response and used the BRAID response surface model to assess the effects of the combination (**Fig.3A**; Supplementary Table S1; ref. 13). In this mathematical model, kappa value indicates the nature of the drug interaction (zero indicates additivity, whereas positive and negative values imply synergism and antagonism, respectively) and IAE_{50} value measures the efficacy of the combination at achieving 50% growth inhibition. Combination of JQ1 with ribociclib was synergistic in HD-MB03, with kappa values ranging from 0.11 to 3.64, and was additive in MB002 and the two other PDX models of G3MB (**Fig. 3B**). IAE_{50} values showed that the combination was the most effective in MB002 (**Fig. 3C**). In HD-MB03 cells, JQ1 in combination with ribociclib induced a significant increase of cell death (**Fig. 3D**) and live cells were arrested in G_1 phase of the cell cycle (**Fig. 3E**). Ribociclib treatment was associated with increased expression of MYC and CYCLIN E proteins (**Fig. 3F**). When combined with ribociclib, JQ1 suppressed the expression of both proteins. Cell-cycle arrest was associated with increased $p27^{KIP1}$ (**Fig. 3F**).

Preclinical evaluation of ribociclib, JQ1, and combination

Brain exposure assessment was performed for three BETi: JQ1, birabresib, and pelabresib (Supplementary Table S3). Pelabresib displayed the best brain to plasma ratio, Kpuu, followed by JQ1 and then birabresib that had a very low Kpuu. Among the three BETi, pelabresib had the lowest potency *in vitro* (**Fig. 1C**; Supplementary Fig. S3B). Therefore, we favored the tool compound JQ1. JQ1's Kpuu was 0.448 in non–tumor-bearing mice (Supplementary Table S3), and *in vitro*, it inhibited the four G3MB models with IC_{50} values ranging from 48 to 307 nmol/L after 7 days of treatment (Supplementary Fig. S3B).

To assess the effects of JQ1 therapy as single agent and in combination with ribociclib on G3MB progression *in vivo*, mice were implanted with luciferase positive HD-MB03, MB002, and SJMBG3–12–5950. HD-MB03 cells displayed the higher ribociclib and JQ1 synergy index (i.e., kappa value) whereas MB002 cells had the higher sensitivity to single agents *in vitro*. SJMBG3–12–5950 cells were chosen for their intermediate *in vitro* profile. Mice were dosed daily with vehicle, 100 mg/kg of ribociclib, 50 mg/kg of JQ1, or both drugs together until animals became moribund (**Fig. 4A**). Daily oral administration of ribociclib at 100 mg/kg in mice is clinically relevant (17) whereas daily intraperitoneal administration of JQ1 at 50 mg/kg in mice is widely used in the literature (10, 18). As a single agent, JQ1 did not affect the survival of tumor-bearing compared with vehicle-treated mice (**Fig. 4B–G**, green vs. black lines). BLI measurements confirmed these data (**Fig. 4C**, **E**, and **G**; Supplementary Fig. S4). In contrast, when treated with ribociclib alone, mice bearing HD-MB03 and MB002 had a significant survival advantage compared with vehicle-treated animals (**Fig. 4B** and **D**, red vs. black lines). In both models, treatment with the combination of ribociclib and JQ1 did not improve mouse survival over ribociclib alone and did not affect the survival of SJMBG3–12–5950-bearing mice (**Fig. 4B**, **D**, and **F**, brown vs. red lines).

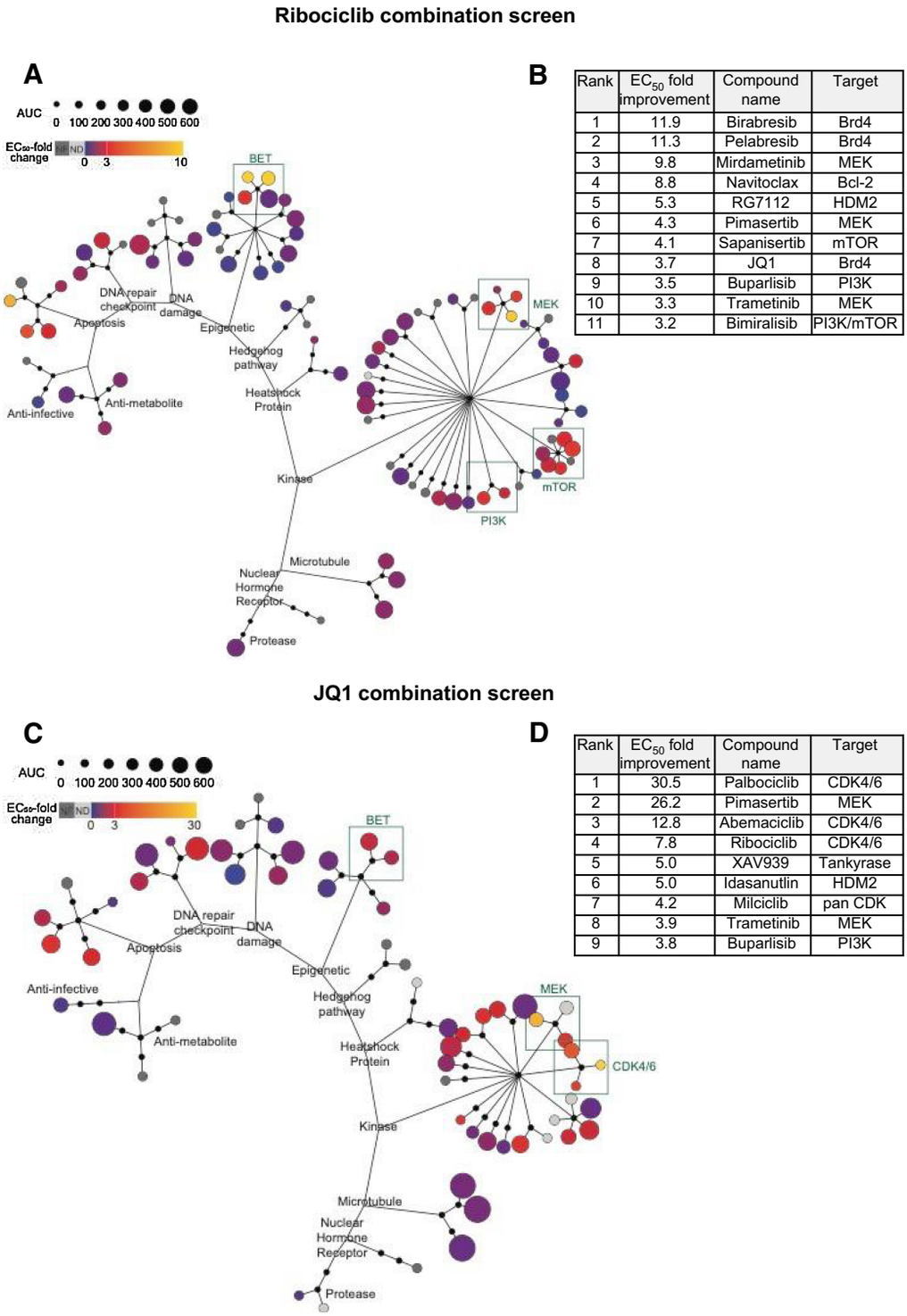

Figure 2.

Anchor-based combination screens in G3MB *in vitro*. **A–D,** In 384-well plate format, HD-MB03 cells treated with DMSO or the anchor at a single concentration in combination with 87 drug partners in dose–response. 7 days after treatment plates submitted to CellTiter Glo assay and fold change (improvement) of drug partners' IC_{50} was computed. **A** and **C,** Each drug partner is represented as a colored circle with potency (AUC) as single agent depicted by size. IC_{50} fold change depicted by color. **B** and **D,** Top ranked drug partners with IC_{50} fold change > 3. **A** and **B,** Ribociclib combination screen using 5 μmol/L of ribociclib and 87 drug partners ($n = 3$ and technical triplicate). **C** and **D,** JQ1 combination screen using 0.132 μmol/L of JQ1 and 59 drug partners ($n = 2$ and technical triplicate). Dose–response curves for top drug partners ± anchor drug are presented in Supplementary Fig. S2. Raw data are presented in Supplementary Table S1.

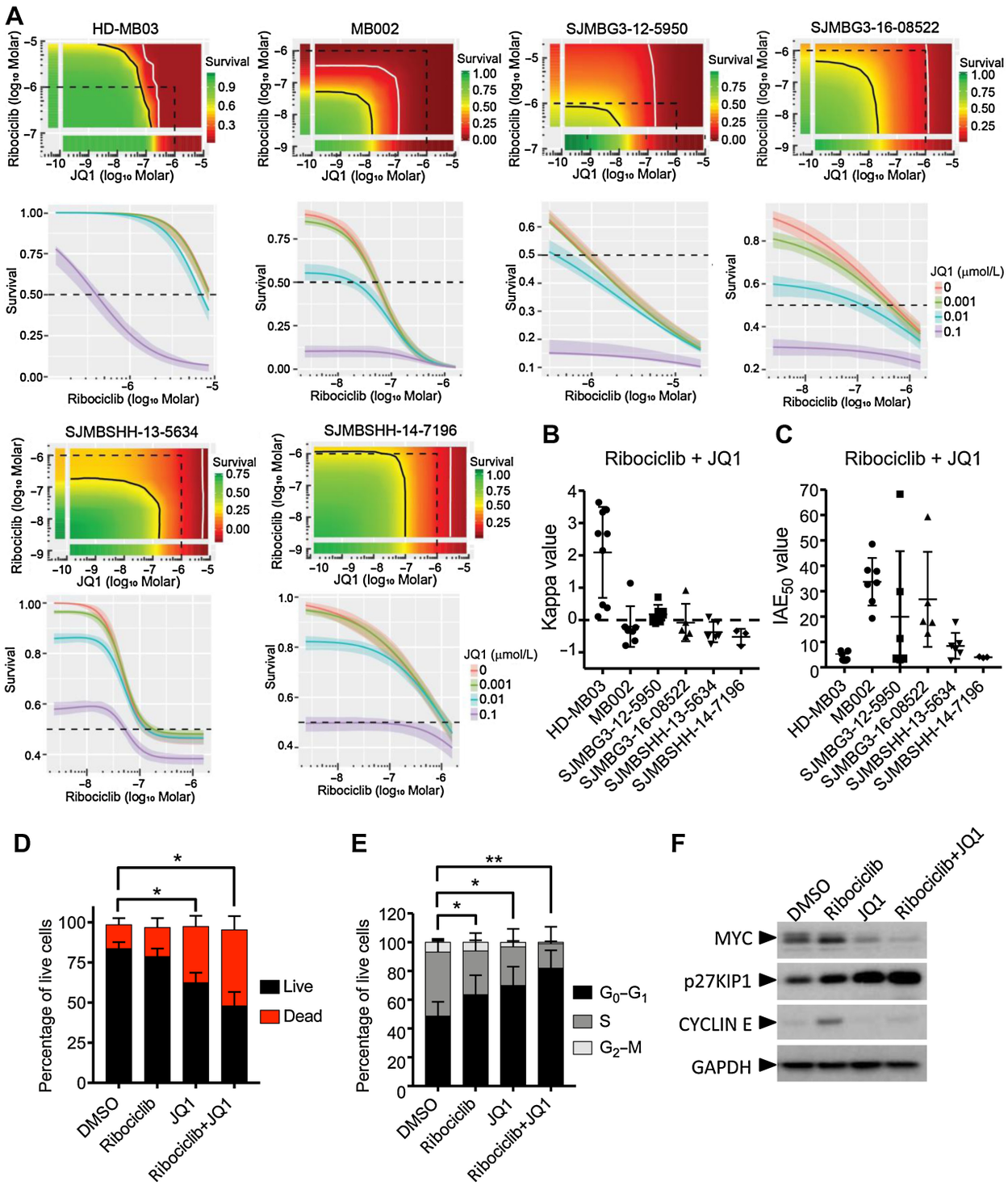

Figure 3.

In vitro combination of ribociclib and JQ1. **A–C,** In 384-well plate format, HD-MB03, MB002, G3MB, and SHHMB PDXs treated with ribociclib and JQ1 in dose–responses for 7 days. Growth inhibition evaluated with CellTiter Glo. Bivariate Response to Additive Interacting Doses (BRAID) response surface model assessing the effect and efficacy of the combination. **A,** Representative response surface model (top) and JQ1 potentiation of ribociclib dose–response (bottom) shown for each model. The red and green color scales indicate low and high proliferation, respectively, relative to vehicle-treated cells. The dotted line encompasses the region in the response surface where each drug is ≤1 μmol/L and shown for reference. The black and white lines are the drug combination isoboles representing 50% and 90% inhibition of cell proliferation, respectively (top). (*Continued on the following page.*)

The JQ1 and ribociclib combination was well tolerated (Supplementary Fig. S5A–S5G). We observed mild leukopenia in mice treated with ribociclib alone or with the combination, as expected from clinical data with CDK4/6i (Supplementary Fig. S5D; ref. 19). In contrast with observations with BETi in clinical trials (20), JQ1 treatment did not induce neutropenia, anemia or thrombocytopenia in MB002-bearing mice (Supplementary Fig. S5E–S5G).

To understand why JQ1 lacked activity *in vivo*, we performed PK studies in non–tumor-bearing mice. After a single dose of JQ1 at 50 mg/kg, the maximal free unbound brain concentration of JQ1 was 100 nmol/L with a 1 hour half-life (**Fig. 4H**). *In vitro,* dose–response washout experiment showed that JQ1 concentration required to affect HD-MB03 cell viability increased dramatically at shorter exposure times (**Fig. 4I**). At 1 hour exposure, corresponding to JQ1 *in vivo* half life, the IC_{50} value was above 2 μmol/L (**Fig. 4I**). Such high and sustained concentrations of JQ1 were unachievable in the brain due to its rapid clearance *in vivo* explaining the lack of efficacy in suppressing tumor growth.

Ribociclib synergizes with the PI3K/mTORi paxalisib to inhibit G3MB and SHHMB proliferation *in vitro*

Whereas brain penetration is variable among all existing PI3K/mTORi, paxalisib (GDC-0084) was specifically designed for brain penetration and has an excellent brain to plasma ratio (21, 22). We combined ribociclib and paxalisib in dose–response and analyzed the data using the BRAID response surface model (**Fig. 5A**; Supplementary Table S1). Kappa values, ranging from 0.5 to 5, revealed synergistic interaction between the two drugs in all G3MB and SHHMB PDXs (**Fig. 5B**). IAE_{50} values ranged from 2 to 30 with SJMBSHH-14–7196 and MB002 being the least and most sensitive models, respectively (**Fig. 5C**). Drug combination in HD-MB03 cells significantly increased cell death (**Fig. 5D**) and induced cell-cycle arrest in G_1 phase (**Fig. 5E**). Unlike JQ1, paxalisib did not suppress the increase of MYC protein expression induced by ribociclib. However, it was associated with a lower level of CYCLIN E protein and an increase of $p27^{KIP1}$ compared with ribociclib alone (**Fig. 5F**).

Preclinical evaluation of ribociclib, paxalisib, and combination *in vivo*

In adult patients, paxalisib PK data endorsed once a day dosing schedule with a maximum tolerated dose of 45 mg/d (23). To identify a suitable dose of paxalisib when combined with ribociclib, non–tumor-bearing mice were treated with 5, 10 or 15 mg/kg of paxalisib and 100 mg/kg of ribociclib daily for 3 weeks (Supplementary Fig. S6A–S6H). Although 15 mg/kg of paxalisib was well tolerated as a single agent, except for inducing hyperglycemia, mice receiving ribociclib and paxalisib at 15 mg/kg experienced acute body weight loss and had to be euthanized on day 8. Blood work revealed leukopenia, neutropenia, anemia thrombocytopenia, and increased aspartate transaminase (AST) levels, but no increase of alanine transaminase (ALT; Supplementary Fig. S6B–S6G). 10 mg/kg of paxalisib given daily proved to be well tolerated for 3 weeks in combination with ribociclib in non–tumor-bearing mice (Supplementary Fig. S6A–S6H). A study to assess the PK drug interaction potential of paxalisib and ribociclib combination was conducted in mice and previously reported (24). Ribociclib, identified as "DrugX," and paxalisib did not demonstrate a significant PK interaction, with the plasma AUCs of each agent remaining within 0.8 to 1.2-fold versus monotherapy (paxalisib $P = 0.158$, ribociclib $P = 0.472$).

Mice harboring HD-MB03, MB002, and SJMBSHH-13–5634, with good synergy score (kappa value) and/or good *in vitro* single-agent activity, were treated with vehicle, 100 mg/kg of ribociclib, 10 mg/kg of paxalisib or the combined formulation until animals became moribund (**Fig. 6A**; Supplementary Fig. S7). In all three models, paxalisib, as a single agent, had no effect on mouse survival (**Fig. 6B–G**, green vs. black lines; Supplementary Fig. S7A–S7F). In contrast, ribociclib increased the survival of mice bearing MB002 (**Fig. 6D** and **E**, red vs. black lines; **Fig. 4D** and **E**) and SJMBSHH-13–5634 (**Fig. 6F** and **G**, red vs. black lines). Mice treated with the drug combination exhibited improved survival over vehicle with a 12, 23, and 25-day increase, respectively (**Fig. 6B–G**, blue vs. black lines). Despite an apparent increased of the median survival of HD-MB03 and MB002-bearing mice treated with the combination versus those treated with ribociclib alone, this difference did not reach significance (**Fig. 6B–E**, red vs. blue lines). In SJMBSHH-13–5634–bearing mice, combination and ribociclib alone treatments were associated with the same survival profile (**Fig. 6F** and **G**, red vs. blue lines). Tumor burden was concordant with survival (**Fig. 6C**, **E**, and **G**; Supplementary Fig. S7). In MB002-bearing mice, the combination treatment significantly delayed tumor burden and spinal metastasis (Supplementary Fig. S7G and S7H).

Mice treated with paxalisib alone or the combination underwent severe weight loss and had poor body condition, including being hunched and emaciated that was not observed to that extent in other treatment groups (Supplementary Fig. S8A–S8C). Blood work on HD-MB03-bearing mice treated with the combination showed mild leukopenia without neutropenia, anemia, increased liver transaminases ALT and AST and hyperglycemia but no thrombocytopenia (Supplementary Fig. S8D–S8J). Similar data were observed in SJMBSHH-13–5634–bearing mice treated with ribociclib and paxalisib except that anemia and increase liver transaminases were not detected (Supplementary Fig. S8K–S8Q).

Molecular analysis of tumors treated with ribociclib and paxalisib

To investigate the molecular response to treatment in G3MB and SHHMB models, we analyzed gene expression profiles of tumors harvested at endpoint (**Fig. 4**) and compared these profiles between tumors treated with ribociclib, paxalisib or the combination and those treated with vehicle. Gene set enrichment analysis (GSEA) showed five highly downregulated gene sets common in the three combination-treated tumor models, including E2F targets and PI3K–AKT–MTORC1 signaling consistent with CDK4/6 (5) and PI3K/mTOR inhibition, as well as G_2–M checkpoint, MYC targets, and Glycolysis gene sets (**Fig. 7A**; Supplementary Table S4). Many of

(*Continued.*) Endpoints of these lines are driven by the potency of each drug as single agent. These lines will curve inward toward the origin for synergistic combinations and bow outward away from the origin for antagonistic combinations. **B,** Kappa values ($n = 3$–9), type of interaction between the two combined drugs. When kappa is close to zero, the combination is additive, whereas positive and negative values imply synergism and antagonism, respectively. **C,** IAE_{50} values ($n = 3$–9), measure of the efficacy at achieving 50% growth inhibition. BRAID data are available in Supplementary Table S1. **D–F,** HD-MB03 cells treated with DMSO, 5 μmol/L of ribociclib, 0.3 μmol/L of JQ1 or the combination for 72 hours. **D,** Dead and apoptotic cells stained with Annexin V-APC reagent and (**E**) DNA content analyzed on permeabilized nuclei using propidium iodide by flow cytometry. Statistical analyses performed on the percentage of AnnexinV positive cells (dead; **D**) and on the percentage of cells in G_0–G_1 in the cell cycle (**E**; Mann and Whitney test, $n = 4$ and $n = 6$, respectively). **F,** MYC, CYCLIN E, $p27^{KIP1}$, and GAPDH expression analyzed by immunoblotting ($n = 3$).

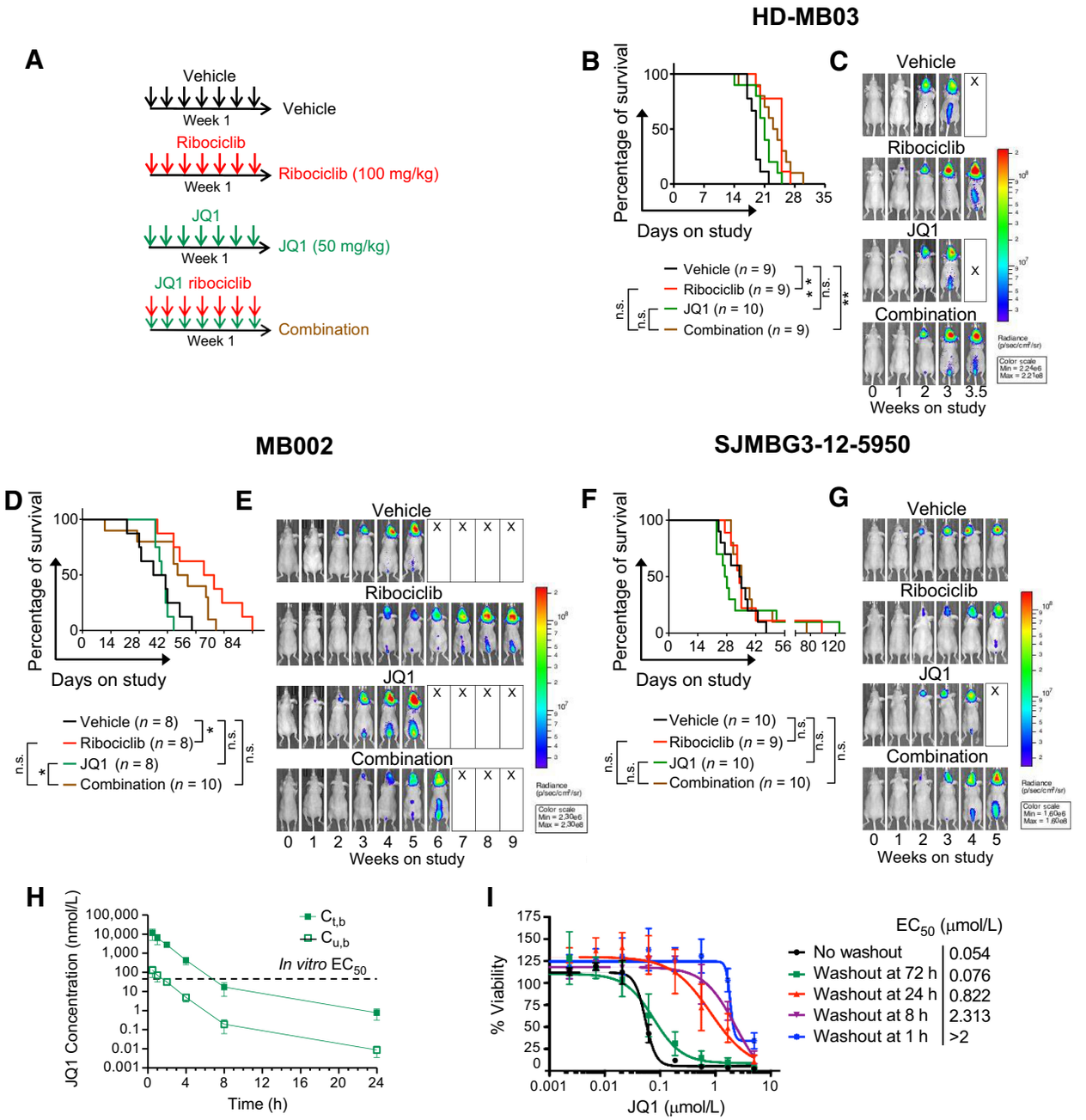

Figure 4.

Treatment with ribociclib, JQ1, and combination in G3MB-bearing mice *in vivo*. **A,** Treatment schedule after enrollment. **B–G,** Mice bearing PDXs HD-MB03 (**B** and **C**) MB002 (**D** and **E**) or SJMBG3–12–5950 (**F** and **G**) tumor cells treated with vehicle (black lines), ribociclib (100 mg/kg, continuous daily by oral gavage, red lines), JQ1 [50 mg/kg, continuous daily intraperitoneal (IP), green lines], or the combination (brown lines) until moribund. **B, D,** and **F,** Kaplan–Meier survival plots for all treatment groups. Comparison between treatment groups using the log-rank test adjusted for multiple comparisons [not significant (n.s.), adjusted *, $P \leq 0.05$ and adjusted **, $P \leq 0.01$]. Median survival for HD-MB03–bearing mice in days: Vehicle: 19; ribociclib: 25; JQ1: 21; combination: 23.5; ribociclib versus vehicle: adjusted $P = 0.0015$. Median survival for MB002-bearing mice in days: vehicle: 38; ribociclib: 62.5; JQ1: 40; combination: 49.5; ribociclib versus vehicle treated: Adjusted $P = 0.0203$. Median survival for SJMBG3–12–5950–bearing mice in days: Vehicle: 33.5; ribociclib: 34.5; JQ1: 27.5; combination: 35. Mice were imaged twice weekly by bioluminescence imaging (BLI). **C, E,** and **G,** BLI pictures at different time points from enrollment through moribund stage represented for one mouse per treatment group. Mice were selected on the basis of tumor and spinal growth median behavior. For BLI signal curves see Supplementary Fig. S4. **H,** JQ1 pharmacokinetic study in non–tumor-bearing mice after a single dose of 50 mg/kg delivered via IP. Ct,b: total brain concentration; Cu,b: unbound brain concentration. Dashed line represents *in vitro* IC_{50} value of JQ1 in MB002 cells (the most sensitive model *in vitro*). **I,** JQ1 washout study. HD-MB03 cells treated with JQ1 and the cell medium removed and replaced with fresh medium at different time points after treatment. Viability evaluated after 7 days using CellTiter Glo ($n = 3$ and technical duplicate for each).

the same gene sets were significantly downregulated in single-agent treatment groups in comparison with vehicle but they showed a more variable response than the combination group (**Fig. 7A**).

We looked at DEGs between ribociclib, paxalisib or the combination versus vehicle-treated tumors and their overlap (**Fig. 7B**) and performed an unsupervised cluster analysis of the top 100 DEGs call from each analysis (Supplementary Fig. S9A). In all three models, the combination of ribociclib and paxalisib was associated with a higher number of DEGs than single agents (**Fig. 7B**). Consistent with the observation that ribociclib was the dominant partner in the combination treatment, samples from the ribociclib and combination treatments clustered well together for both MB002 and SJMBSHH-13–5634 (Supplementary Fig. S9A). Because survival of mice treated with the combination was not significantly different from those treated with ribociclib alone (**Fig. 6**), we investigated the impact of paxalisib in the combination-treated tumors by comparing DEGs between combination and ribociclib-only treated tumor samples (**Fig. 7C**). No DEGs were found in SJMBSHH-13–5634 tumors (FDR < 0.05), indicating that paxalisib had little effect on gene expression when combined with ribociclib (**Fig. 7C**). In contrast, the same comparison in HD-MB03 showed the greatest number of DEGs (2,791 DEGs, FDR<0.05), indicating a synergistic effect (**Fig. 7C**). GSEA analysis of these DEGs between combination and ribociclib-treated tumors showed enrichment of MYC targets and PI3K–AKT–MTORC1 signaling gene sets in HD-MB03 and MB002 (**Fig. 7C**; Supplementary Tables S5 and S6). We performed a Kruskal–Wallis test and subsequent *post hoc* multiple pairwise comparison of the PI3K–AKT–MTORC1 signaling pathway using gene set variation analysis scores of treated samples from each medulloblastoma model (Kruskal–Wallis $P = 0.002$, 0.007, and 0.019 for HD-MB03, MB002, and SJMBSHH-13–5634, respectively; **Fig. 7D**). We found a significant downregulation of the PI3K–AKT–MTORC1 signaling pathway in HD-MB03 tumors treated with the combination of ribociclib and PI3K–mTORi in comparison with ribociclib alone (**Fig. 7D**, FDR < 0.05). The same downregulation was found in MB002 tumors treated with the drug combination, although it was not significant. We saw no difference in the PI3K–mTOR pathway in SJMBSHH-13–5634 when comparing tumors treated with ribociclib alone or in combination with the PI3K–mTORi. Despite inhibition of the PI3K/AKT/mTOR signaling pathway at the molecular level (**Fig. 7A** and **D**), paxalisib did not significantly impact tumor growth in any of the three models (**Fig. 6**).

To examine potential discrepancies in PI3K–AKT–MTORC1 signaling basal activity between *in vitro* and *in vivo*, we compared gene expression in HD-MB03 tumorspheres (*in vitro*) and tumor treated with vehicle (*in vivo*). Using GSEA, HD-MB03 grown *in vitro* showed significant upregulation in PI3K–AKT–MTORC1 signaling compared with *in vivo* (**Fig. 7E**).

To investigate the extent of gene expression changes in treated tumors that grew while on treatment, we compared them with the untreated medulloblastoma PDXs from the previously generated four medulloblastoma subgroups (11). As visualized by t-distributed Stochastic Neighbor Embedding (t-SNE plot, Supplementary Fig. S9B), all treated and untreated tumors primarily clustered by tumor model and by subgroup. Genetic alterations, including gene amplification are thought to confer intrinsic and acquired resistance to PI3K/mTOR and CDK4/6 inhibitors (25–27). Several genes involved in CDK4/6i resistance were overexpressed in the tumors treated with the combination of ribociclib and paxalisib or ribociclib alone versus vehicle, including *CCND1, CCND2, CDK6, ERBB2* (**Fig. 7F**). Genes known to be associated with PI3K/mTORi resistance were dysregulated in the tumors treated with the single agents or the combination when compared with vehicle, including *EIF4EBP1, IGF1R, IRS1, IRS2, SGK1, PDGFR, MET*, and *HGF* (**Fig. 7F**).

Discussion

Although standard of care is effective in patients with medulloblastoma with low-risk tumors, relapses often occur for which there are little treatment options. To identify novel targeted therapies, we performed *in vitro* HTS. We reasoned that freshly dissociated tumor cells would best recapitulate original tumors and be better suited to identify drug vulnerabilities compared with established cell lines. Freshly dissociated cells from G3 and SHH PDX tumors grew transiently in 384-well plate, in agreement with a recent report showing the feasibility of using dissociated cells from medulloblastoma PDXs for drug screens (28). Single agents HTS showed inhibitors of CDK4/6, BET, CDK7, CDK9, PI3K/mTOR, HDAC, DNA topoisomerase, CHK, microtubule, Aurora kinases, PLK1 and gemcitabine inhibited proliferation of a panel of human medulloblastoma tumor cells *in vitro*, as previously reported (29–31). The CDK4/6i ribociclib inhibited tumor progression in one model of G3MB and one model of SHHMB and was well tolerated *in vivo*. Those two sensitive medulloblastoma models were also the most sensitive to ribociclib *in vitro*, suggesting a good correlation between *in vitro* and *in vivo*. This adds to a growing body of evidence that CDK4/6 inhibition is a promising new approach to treat MBs (4, 32). Because of their cytostatic effect, CDK4/6i are not expected to lead to clinical benefit as single agents. Numerous trials are evaluating CDK4/6 inhibitors in combination with other targeted agents, chemotherapy, or immunotherapy for different cancer types (33). In MB, ribociclib is currently evaluated in the clinic in combination with the smoothened inhibitor, sonidegib or the MEKi, trametinib for SHH subgroup or gemcitabine for G3 and G4 subgroups (SJDAWN: NCT03434262). We found that E2F targets were downregulated in tumors at endpoint after treatment with ribociclib compared with those treated with vehicle, suggesting that *in viv*o CDK4/6 inhibition remains potent over time. However, mice succumbed to their tumors while on treatment. Notably, *CCND1*, *CCND2*, *CDK6*, and *ERBB2 (HER2)* were upregulated in these tumors and might be responsible for the lack of durable response to ribociclib as seen with acquired resistance in HR^+ breast cancers (25).

BETi, JQ1, birabresib and pelabresib showed activity in all medulloblastoma models *in vitro*. By regulating the positive transcription elongation factor beta (P-TEFb) complex, BRD4 is a promising target for MYC-driven cancers (34). MYC and MYCN-driven G3MB and SHHMB were previously found to be sensitive to JQ1 *in vitro* (10, 18, 35, 36). However, in our studies, continuous daily administration of JQ1 at 50 mg/kg had no effect on tumor growth or survival of mice bearing intracranial *MYC*-amplified G3MBs. The measured brain exposure in non–tumor-bearing mice and *in vitro* washout experiments demonstrated that due to low unbound brain concentration and rapid clearance, JQ1 was unable to exert antitumoral activity *in vivo*. We note that these findings are in contrast with an earlier reported *in vivo* study that demonstrated JQ1 activity as single agent in the intracranial *MYC*- amplified G3MB model MB002 (10). Interestingly, more recently reported studies found JQ1 activity only modest or even absent in G3MB models (18, 35). We hypothesize that these discrepancies between studies might arise from differences in PK profile of JQ1 in mice strains used by different investigators. Importantly, previous studies used an intensified schedule of treatment (twice a day) to show JQ1 activity on biomarkers, including MYC protein in preclinical models of medulloblastoma versus the standard tolerated daily dose (10). Among the other

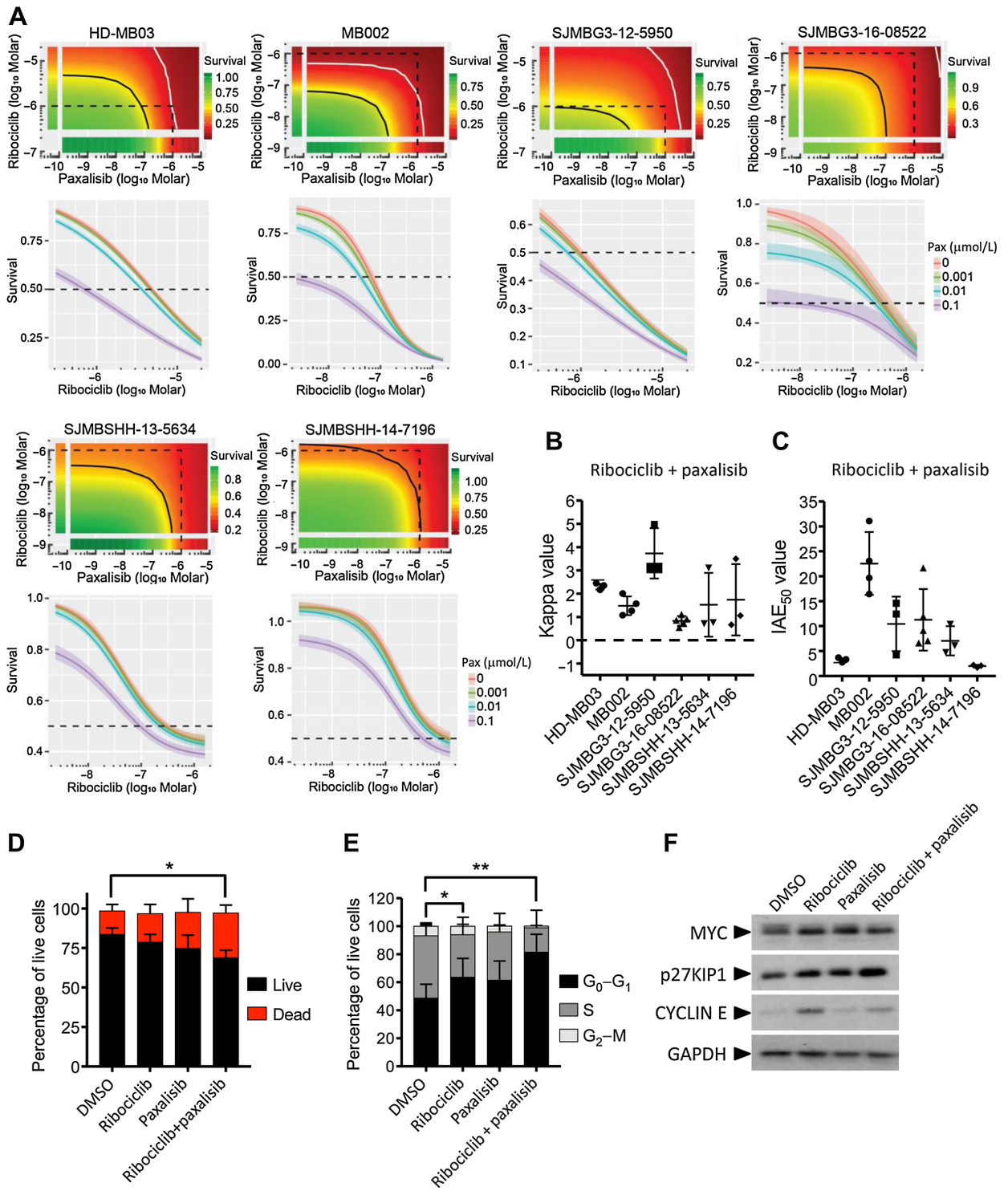

Figure 5.

In vitro combination of ribociclib and paxalisib. **A** and **B,** In 384-well plate format, HD-MB03, MB002, G3MB, and SHHMB PDXs treated with ribociclib and paxalisib (GDC-0084) in dose–response curves for 7 days and growth inhibition evaluated using CellTiter Glo. Bivariate Response to Additive Interacting Doses (BRAID) response surface model assessed the effect and efficacy of the combination. **A,** Representative response surface model (top) and paxalisib potentiation of ribociclib dose response (bottom) shown for each model. The red and green color scales indicate low and high proliferation, respectively, relative to vehicle-treated cells. The dotted line encompasses the region in the response surface where each drug is ≤1 μmol/L and shown for reference. (*Continued on the following page.*)

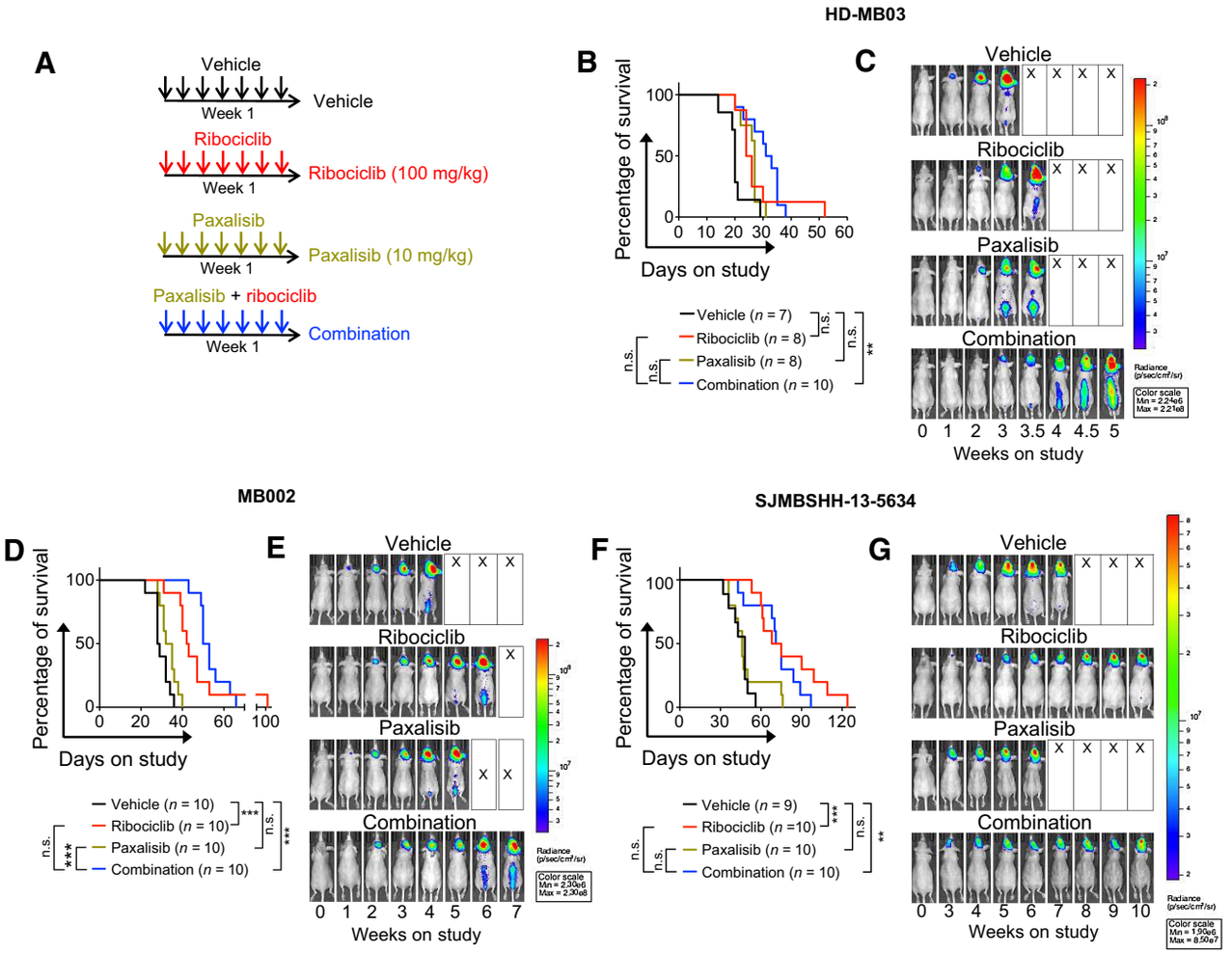

Figure 6.

Ribociclib and paxalisib treatment of G3MB and SHHMB *in vivo*. **A,** Treatment schedule after enrollment. **B–G,** Mice bearing PDXs HD-MB03 (**B** and **C**) MB002 (**D** and **E**) or SJMBSHH-13–5634 (**F** and **G**) tumor cells treated with vehicle (black lines), ribociclib (100 mg/kg, continuous daily by oral gavage (OG), red lines), paxalisib (10 mg/kg, continuous daily OG, green lines), or the combined formulation (continuous daily OG, blue lines) until moribund. (B, D, F) Kaplan-Meier survival plots for all treatment groups. Comparison between treatment groups using log-rank test adjusted for multiple comparisons [not significant (n.s.), adjusted *, $P \leq 0.05$, adjusted **, $P \leq 0.01$, and adjusted ***, $P \leq 0.001$]. Median survival for HD-MB03–bearing mice in days: Vehicle: 20; ribociclib: 25; paxalisib: 27; combination: 32; ribociclib versus vehicle: adjusted $P = 0.0795$; combination versus vehicle: adjusted $P = 0.003$; combination versus ribociclib: adjusted $P = 0.3674$. Median survival for MB002-bearing mice in days: Vehicle: 28.5; ribociclib: 42.5; paxalisib: 33.5; combination: 51.5; ribociclib versus vehicle: adjusted $P = 0.0005$; combination versus vehicle: adjusted $P = 0.0005$; combination versus ribociclib: adjusted $P = 0.1456$. Median survival for SJMBSHH-13–5634-bearing mice in days: vehicle: 48; ribociclib: 71.5; paxalisib: 46; combination: 73; ribociclib versus vehicle: Adjusted $P = 0.0005$; combination versus vehicle: Adjusted $P = 0.0028$; combination versus ribociclib: Adjusted $P = 0.4886$. Mice were imaged twice weekly by bioluminescence imaging (BLI). **C, E,** and **G,** BLI pictures at different time points from enrollment through moribund stage represented for one mouse per treatment group. Mice selected on the basis of tumor and spinal growth median behavior. For BLI signal curves see Supplementary Fig. S7.

(*Continued.*) The black and white lines are the drug combination isoboles representing 50% and 90% inhibition of cell proliferation, respectively (top). Endpoints of these lines are driven by the potency of each drug as single agent. These lines will curve inward toward the origin for synergistic combinations and bow outward away from the origin for antagonistic combinations. Note: HD-MB03 cells were more sensitive to ribociclib in this assay due to change in cell density (500 vs. 1,000 cells/well). **B,** Kappa values ($n = 3$–5), type of interaction between the two combined drugs. When kappa is close to zero, the combination is additive, whereas positive and negative values imply synergism and antagonism, respectively. **C,** IAE_{50} values ($n = 3$–5), measure of the efficacy at achieving 50% growth inhibition. BRAID data are available in Supplementary Table S1. **D–F,** HD-MB03 cells treated with DMSO, 5 μmol/L of ribociclib, 0.5 μmol/L of paxalisib or the combination for 72 hours. **D,** Dead and apoptotic cells stained with Annexin V-APC reagent and (**E**) DNA content analyzed on permeabilized nuclei using propidium iodide by flow cytometry. Statistical analyses were performed on the percentage of AnnexinV positive cells (**D**) and on the percentage of cells in G_0–G_1 of the cell cycle (**E**; Mann and Whitney test, $n = 4$ and $n = 6$, respectively). Note: DMSO and ribociclib conditions for **D** and **E** were presented in Supplementary Fig. S3. **F,** MYC, CYCLIN E, $p27^{KIP1}$, and GAPDH expression analyzed by western blot ($n = 3$).

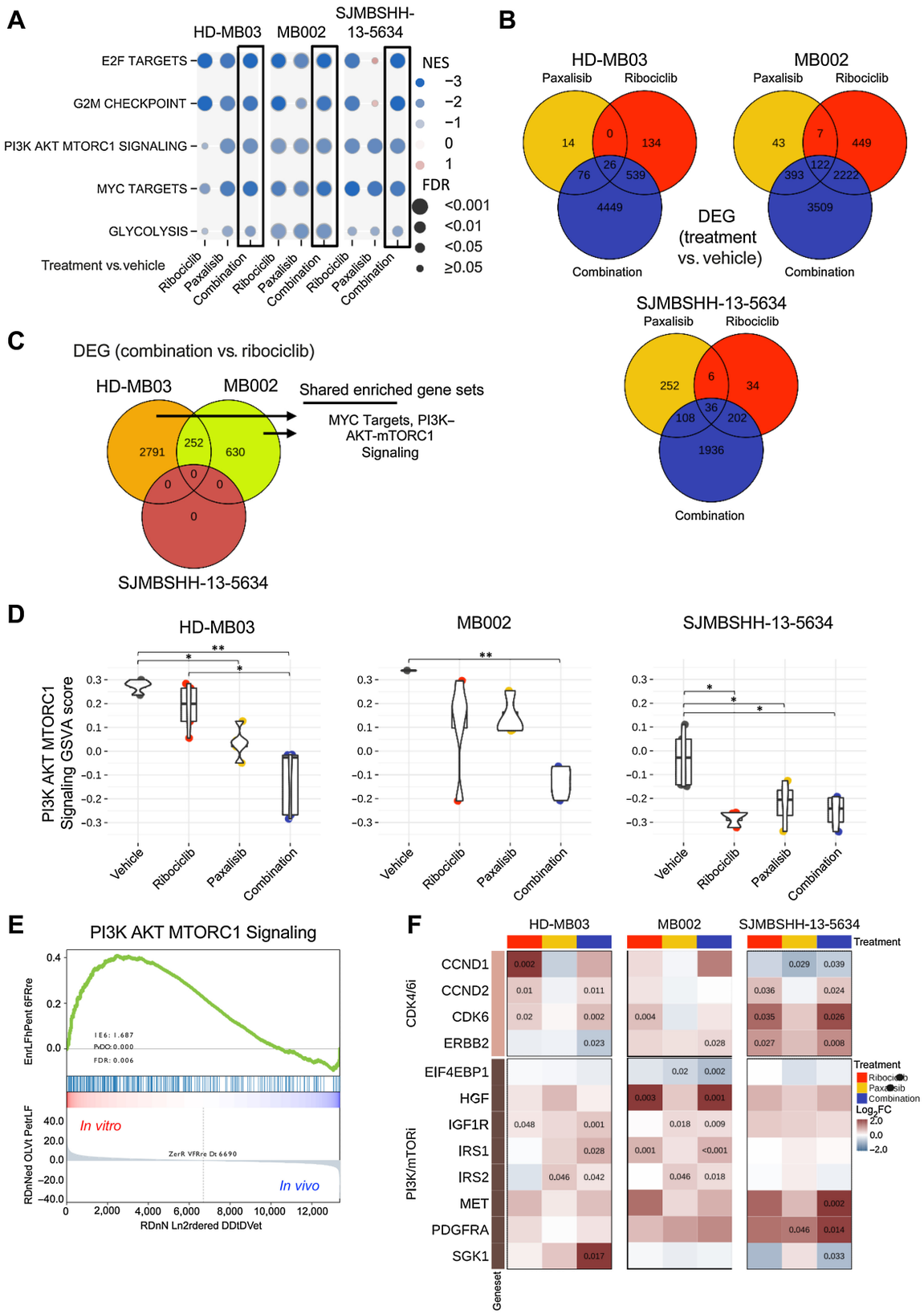
A
HD-MB03
MB002
SJMBSHH-13-5634
E2F TARGETS
G2M CHECKPOINT
PI3K AKT MTORC1 SIGNALING
MYC TARGETS
GLYCOLYSIS
Treatment vs. vehicle
Ribociclib
Paxalisib
Combination
NES
−3
−2
−1
0
1
FDR
<0.001
<0.01
<0.05
≥0.05
B
HD-MB03
Paxalisib
Ribociclib
Combination
14
0
134
76
26
539
4449
MB002
43
7
449
393
122
2222
3509
DEG (treatment vs. vehicle)
SJMBSHH-13-5634
252
6
34
108
36
202
1936
C
DEG (combination vs. ribociclib)
HD-MB03
MB002
SJMBSHH-13-5634
2791
252
630
0
0
0
0
Shared enriched gene sets
MYC Targets, PI3K–AKT-mTORC1 Signaling
D
HD-MB03
MB002
SJMBSHH-13-5634
PI3K AKT MTORC1 Signaling GSVA score
Vehicle
Ribociclib
Paxalisib
Combination
E
PI3K AKT MTORC1 Signaling
In vitro
In vivo
RDnN Ln2rdered DDtDVet
F
HD-MB03
MB002
SJMBSHH-13-5634
Treatment
CDK4/6i
PI3K/mTORi
CCND1
CCND2
CDK6
ERBB2
EIF4EBP1
HGF
IGF1R
IRS1
IRS2
MET
PDGFRA
SGK1
Geneset
Log2FC

BETi that we tested, birabresib was not brain penetrant (Kpuu of 0.028) and pelabresib was not sufficiently potent *in vitro* (3-fold higher IC_{50} value compared with JQ1). In aggregate, our data suggest that BET inhibitors with more optimal central nervous system (CNS) PK profile should be tested with CDK4/6i to assess the potential therapeutic benefit of this combination. However, despite the great promises raising from early preclinical studies, BETi efficacy remains to be validated in the clinic (20). Among the novel strategies to inhibit BET proteins, proteolysis-targeting chimera is an area of intense investigation (37, 38). With the emerging roles of BET proteins in the CNS (39), it will be interesting to see if BET inhibition or degradation delivers effective and safe clinical treatments.

To identify novel drug combinations that inhibit medulloblastoma proliferation, we devised an anchor combination drug screen in which ribociclib was used at the IC_{20} value whereas the partner drugs were used in dose–response. We identified three BET and three PI3K/mTOR inhibitors as potentiating drug partners for ribociclib *in vitro*. We then used JQ1 as the anchor against a panel of drugs in dose–response and again found the three CDK4/6 and several PI3K/mTOR inhibitors. The potentiation between ribociclib and BETi seen *in vitro* could be mediated by the modulation of MYC protein expression. BETi were previously shown to suppress MYC expression and tumor proliferation in several cancers, including medulloblastoma (10, 40). We found that MYC was upregulated at the protein level after treatment with ribociclib in HD-MB03 cells. Loss or inhibition of CDK4/6 led to MYC addiction and metabolic reprogramming in colorectal cancer cell lines (41), and MYC overexpression conferred resistance to CDK4/6 inhibitors in breast cancer cells (42). Combination of JQ1 and ribociclib potently represses MYC expression and blocks the induction of its expression observed after ribociclib treatment in HD-MB03 cells *in vitro*. Potentiation between BETi and CDK4/6i was previously shown in NUT midline carcinoma (43), breast cancer (44), and G3MBs (18, 35). Although *in vitro* data in the different cancer models are compelling, this combination induces only a short survival improvement in intracranial G3MBs models (18).

PI3K–mTORi were synergistic with ribociclib in G3MB and SHHMB *in vitro*. Multiple preclinical studies in other tumor models showed the advantage of combining CDK4/6i and PI3K/mTORi (25, 33, 45). However, treatment of mice bearing intracranial MBs with paxalisib, a PI3K/mTORi, as single agent or in combination with ribociclib, did not significantly improve survival compared with ribociclib alone. Despite being a drug specifically designed for brain tumors, at a dose superior to the dose needed for on target effect in CD-1 nude mouse brain (24), paxalisib failed to show efficacy in medulloblastoma models *in vivo*. Molecularly, paxalisib downregulated PI3K–AKT–MTORC1 signaling, as expected, and was acting synergistically with ribociclib in HD-MB03. However, in MB002 and SJMBSHH-13–5634 the combination showed a modest to absent effect in comparison with ribociclib alone. This might be due to ribociclib downregulating PI3K–AKT–MTORC1 signaling on its own in these two models. Notably, the PI3K–AKT–MTORC1 signaling gene set was downregulated *in vivo* compared with *in vitro* in HD-MB03 cells. This could be correlated to a lower dependency to this pathway *in vivo* compared with *in vitro* in the medulloblastoma models tested. Aberrant expression of members of the PI3K/AKT/mTOR signaling pathways are described previously in human MBs and are associated with poor prognoses (46, 47). The PI3K inhibitor, BKM120, was active in mouse and human G3MB models (31). However, the preclinical data supporting this class of compounds are limited for MB. Genes associated with resistance to PI3K/mTORi were upregulated in the tumors treated with ribociclib, paxalisib, and the combination in comparison with vehicle-treated tumors, including *IGF1R*, *IRS1*, *IRS2*, *MET*, and *SGK1* (26, 27) that might explain the insignificant impact of paxalisib in these tumors. The full benefit of the combination with CDK4/6i and PI3K/mTORi might be unlocked when combined with standard of care (45) or tested in immune-competent mice with immune checkpoint blockade therapy (48). Paxalisib is currently evaluated in children with brain tumors in combination with radiation therapy in a Phase I clinical trial (SJPI3K and NCT03696355).

The major limitation of using PI3K/mTORi is their toxicity profile. Despite tolerability of the combination of ribociclib and paxalisib in non–tumor-bearing animals for 3 weeks, tumor-bearing animals experienced hyperglycemia, weight loss, and elevation of transaminases, common side effects in patients treated with PI3K/mTORi (23, 49).

In vitro drug screens remain a valuable tool to identify novel drug combinations in MBs and other cancers. Preclinical studies using intracranial/orthotopic medulloblastoma models are essential to evaluate new therapeutic modalities before being tested in clinical trial. We identified BETi and PI3K/mTORi as drug partners that potentiate ribociclib *in vitro* but both combinations failed to provide survival advantage in mice bearing G3MB or SHHMB compared with ribociclib alone. Our data suggest that JQ1 brain concentration were insufficient for *in vivo* activity and that other BETi with better brain PK profile should be evaluated in combination with CDK4/6i in MB. Despite good *in vitro* activity many drugs fail in preclinical models of brain tumors due to insufficient drug concentration in the brain, altered signaling pathways *in vitro,* cellular heterogeneity, or other mechanisms (28, 50–53) illustrating the complexity of translating *in vitro* findings *in vivo* especially in the CNS space. A better understanding of frequently observed discrepancy between *in vitro* and *in vivo* activity will be necessary to improve the success of discovering and developing new therapies for the treatment of MBs.

Figure 7.

Gene expression analysis of tumors treated with ribociclib and paxalisib. RNAs from HD-MB03, MB002, and SJMBSHH-13–5634 tumors, from the preclinical studies presented on **Fig. 6**, were sequenced. Gene set enrichment analysis (GSEA) and differential expressed gene (DEG) analysis performed between tumors treated with ribociclib, paxalisib or combination versus vehicle. **A,** Plot showing the Normalized Enrichment Score (NES, circles in color) and FDR (circles size) of the gene sets found to be significantly depleted in each of the three medulloblastoma models when comparing combination versus vehicle-treated tumors (black boxes). Other comparisons include ribociclib or paxalisib versus vehicle-treated tumors. GSEA data are presented in Supplementary Table S4. **B,** Venn diagram of DEGs between each treatment (ribociclib-only, paxalisib-only, and the combination) and vehicle for each model (FDR < 0.05). **C,** Venn diagram of DEGs between combination and ribociclib-treated tumors in each model. Enriched gene set term analysis of HD-MB02 and MB002 models DEGs, run separately, showed two shared gene sets, including MYC Targets and PI3K–AKT–MTORC1 signaling. Data are presented in Supplementary Tables S5 and S6. **D,** Multiple pairwise comparison of PI3K–AKT–MTORC1 signaling pathway between treatments for each medulloblastoma model. Gene set variation scores of PI3K–AKT–MTORC1 pathway genes calculated for each sample and compared with a Kruskal–Wallis test, followed by a *post hoc* Dunn test. Only significant FDR adjusted *P* comparisons are shown (*, $P < 0.05$; **, $P < 0.01$). **E,** GSEA of PI3K–AKT–MTORC1 signaling with HD-MB03 cell line (*in vitro*) and HD-MB03 vehicle treated tumors (*in vivo*). **F,** Heatmap with $\log_2$ fold change ($\log_2$FC) between ribociclib, paxalisib or combination versus the vehicle group for genes known to be involved in resistance to CDK4/6 and PI3K/mTOR inhibitors. Adjusted *P* values are indicated for significant DEGs.

Authors' Disclosures

J. Min reports to be an Amgen stockholder. Z. Rankovic reports receiving consultation fees from Revolution Medicine, Orum Therapeutics, and Nurada Therapeutic, and is Eli Lilly stockholder. No disclosures were reported by the other authors.

Disclaimer

The content is solely the responsibility of the authors and does not necessarily represent the official views of the National Institutes of Health.

Authors' Contributions

B. Jonchere: Conceptualization, data curation, formal analysis, validation, investigation, visualization, methodology, writing–original draft, writing–review and editing. **J. Williams:** Data curation, software, formal analysis, validation, visualization, methodology, writing–review and editing. **F. Zindy:** Investigation, writing–review and editing. **J. Liu:** Methodology, writing–review and editing. **S. Robinson:** Investigation, writing–review and editing. **D.M. Farmer:** Investigation, writing–review and editing. **J. Min:** Conceptualization, methodology. **L. Yang:** Formal analysis, investigation, visualization, methodology, writing–review and editing. **J.L. Stripay:** Investigation. **Y. Wang:** Methodology. **B.B. Freeman:** Resources, methodology. **J. Yu:** Resources. **A.A. Shelat:** Data curation, software, formal analysis, validation, investigation, visualization, methodology, writing–review and editing. **Z. Rankovic:** Conceptualization, resources, investigation, methodology, writing–review and editing. **M.F. Roussel:** Conceptualization, resources, formal analysis, supervision, funding acquisition, investigation, writing–original draft, project administration, writing–review and editing.

Acknowledgments

We thank Kimberly Shea Mercer, Jose Grenet, Eleonore Bombard, Melissa Johnson and the Center for In Vivo Imaging and Therapeutics (CIVIT), Technical Services, Yong Li, Xiang Fu, the Veterinary Pathology Core, the Core Flow Cytometry and Cell Sorting Shared Resource and the Department of Chemical Biology for excellent technical expertise. We thank Wendy Pierce, Paige Dunphy, and Delira Robbins for project coordination and members of the Roussel/Sherr laboratory for helpful discussions. This research was supported by NIH grants CA-096832 and CA-02165 (to M.F. Roussel) and the American Lebanese Syrian Associated Charity (ALSAC) of St. Jude Children's Research Hospital.

The publication costs of this article were defrayed in part by the payment of publication fees. Therefore, and solely to indicate this fact, this article is hereby marked "advertisement" in accordance with 18 USC Section 1734.

Note

Supplementary data for this article are available at Molecular Cancer Therapeutics Online (http://mct.aacrjournals.org/).

Received November 3, 2021; revised September 15, 2022; accepted October 21, 2022; published first November 1, 2022.

References

1. Schwalbe EC, Lindsey JC, Nakjang S, Crosier S, Smith AJ, Hicks D, et al. Novel molecular subgroups for clinical classification and outcome prediction in childhood medulloblastoma: a cohort study. Lancet Oncol 2017;18:958–71.
2. Hill RM, Kuijper S, Lindsey JC, Petrie K, Schwalbe EC, Barker K, et al. Combined MYC and P53 defects emerge at medulloblastoma relapse and define rapidly progressive, therapeutically targetable disease. Cancer Cell 2015;27:72–84.
3. Northcott PA, Shih DJ, Peacock J, Garzia L, Morrissy AS, Zichner T, et al. Subgroup-specific structural variation across 1,000 medulloblastoma genomes. Nature 2012;488:49–56.
4. Cook Sangar ML, Genovesi LA, Nakamoto MW, Davis MJ, Knobluagh SE, Ji P, et al. Inhibition of CDK4/6 by palbociclib significantly extends survival in medulloblastoma patient-derived xenograft mouse models. Clin Cancer Res 2017;23:5802–13.
5. Sherr CJ, Beach D, Shapiro GI. Targeting CDK4 and CDK6: from discovery to therapy. Cancer Discov 2016;6:353–67.
6. Schettini F, Giudici F, Giuliano M, Cristofanilli M, Arpino G, Del Mastro L, et al. Overall survival of CDK4/6-inhibitor-based treatments in clinically relevant subgroups of metastatic breast cancer: systematic review and meta-analysis. J Natl Cancer Inst 2020;112:1089–97.
7. Patel YT, Davis A, Baker SJ, Campagne O, Stewart CF. CNS penetration of the CDK4/6 inhibitor ribociclib in non-tumor bearing mice and mice bearing pediatric brain tumors. Cancer Chemother Pharmacol 2019;84:447–52.
8. Delmore JE, Issa GC, Lemieux ME, Rahl PB, Shi J, Jacobs HM, et al. BET bromodomain inhibition as a therapeutic strategy to target c-Myc. Cell 2011;146:904–17.
9. Milde T, Lodrini M, Savelyeva L, Korshunov A, Kool M, Brueckner LM, et al. HD-MB03 is a novel Group 3 medulloblastoma model demonstrating sensitivity to histone deacetylase inhibitor treatment. J Neurooncol 2012;110:335–48.
10. Bandopadhayay P, Bergthold G, Nguyen B, Schubert S, Gholamin S, Tang Y, et al. BET bromodomain inhibition of MYC-amplified medulloblastoma. Clin Cancer Res 2014;20:912–25.
11. Smith KS, Xu K, Mercer KS, Boop F, Klimo P, DeCupyere M, et al. Patient-derived orthotopic xenografts of pediatric brain tumors: a St. Jude resource. Acta Neuropathol 2020;140:209–25.
12. Smith SMC, Bianski BM, Orr BA, Harknett G, Onar-Thomas A, Gilbertson RJ, et al. Preclinical modeling of image-guided craniospinal irradiation for very high-risk medulloblastoma. Int J Radiat Oncol Biol Phys 2019;103:728–37.
13. Twarog NR, Stewart E, Hammill CV, Shelat AA. BRAID: a unifying paradigm for the analysis of combined drug action. Sci Rep 2016;6:25523.
14. Czerniak R. Gender-based differences in pharmacokinetics in laboratory animal models. Int J Toxicol 2001;20:161–3.
15. Waxman DJ, Holloway MG. Sex differences in the expression of hepatic drug metabolizing enzymes. Mol Pharmacol 2009;76:215–28.
16. Ivanov DP, Coyle B, Walker DA, Grabowska AM. In vitro models of medulloblastoma: choosing the right tool for the job. J Biotechnol 2016;236:10–25.
17. Infante JR, Cassier PA, Gerecitano JF, Witteveen PO, Chugh R, Ribrag V, et al. A phase I study of the cyclin-dependent kinase 4/6 inhibitor ribociclib (LEE011) in patients with advanced solid tumors and lymphomas. Clin Cancer Res 2016;22:5696–705.
18. Bandopadhayay P, Piccioni F, O'Rourke R, Ho P, Gonzalez EM, Buchan G, et al. Neuronal differentiation and cell-cycle programs mediate response to BET-bromodomain inhibition in MYC-driven medulloblastoma. Nat Commun 2019;10:2400.
19. Thill M, Schmidt M. Management of adverse events during cyclin-dependent kinase 4/6 (CDK4/6) inhibitor-based treatment in breast cancer. Ther Adv Med Oncol 2018;10:1758835918793326.
20. Sun Y, Han J, Wang Z, Li X, Sun Y, Hu Z. Safety and efficacy of bromodomain and extra-terminal inhibitors for the treatment of hematological malignancies and solid tumors: a systematic study of clinical trials. Front Pharmacol 2021;11:621093.
21. Heffron TP, Ndubaku CO, Salphati L, Alicke B, Cheong J, Drobnick J, et al. Discovery of clinical development candidate GDC-0084, a brain penetrant inhibitor of PI3K and mTOR. ACS Med Chem Lett 2016;7:351–6.
22. Freeman BB III, Yang L, Rankovic Z. Practical approaches to evaluating and optimizing brain exposure in early drug discovery. Eur J Med Chem 2019;182:111643.
23. Wen PY, Cloughesy TF, Olivero AG, Morrissey KM, Wilson TR, Lu X, et al. First-in-human phase I study to evaluate the brain-penetrant PI3K/mTOR inhibitor GDC-0084 in patients with progressive or recurrent high-grade glioma. Clin Cancer Res 2020;26:1820–8.
24. He C, Xu K, Zhu X, Dunphy PS, Gudenas B, Lin W, et al. Patient-derived models recapitulate heterogeneity of molecular signatures and drug response in pediatric high-grade glioma. Nat Commun 2021;12:4089.
25. Jhaveri K, Burris Rd HA, Yap TA, Hamilton E, Rugo HS, Goldman JW, et al. The evolution of cyclin dependent kinase inhibitors in the treatment of cancer. Expert Rev Anticancer Ther 2021;21:1105–24.
26. Formisano L, Napolitano F, Rosa R, D'Amato V, Servetto A, Marciano R, et al. Mechanisms of resistance to mTOR inhibitors. Crit Rev Oncol Hematol 2020;147:102886.
27. Vitale SR, Martorana F, Stella S, Motta G, Inzerilli N, Massimino M, et al. PI3K inhibition in breast cancer: identifying and overcoming different flavors of resistance. Crit Rev Oncol Hematol 2021;162:103334.

28. Rusert JM, Juarez EF, Brabetz S, Jensen J, Garancher A, Chau LQ, et al. Functional precision medicine identifies new therapeutic candidates for medulloblastoma. Cancer Res 2020;80:5393–407.
29. Endersby R, Whitehouse J, Pribnow A, Kuchibhotla M, Hii H, Carline B, et al. Small-molecule screen reveals synergy of cell cycle checkpoint kinase inhibitors with DNA-damaging chemotherapies in medulloblastoma. Sci Transl Med 2021; 13:eaba7401.
30. Morfouace M, Shelat A, Jacus M, Freeman BB III, Turner D, Robinson S, et al. Pemetrexed and gemcitabine as combination therapy for the treatment of Group3 medulloblastoma. Cancer Cell 2014;25:516–29.
31. Pei Y, Liu KW, Wang J, Garancher A, Tao R, Esparza LA, et al. HDAC and PI3K antagonists cooperate to inhibit growth of MYC-driven medulloblastoma. Cancer Cell 2016;29:311–23.
32. Hanaford AR, Archer TC, Price A, Kahlert UD, Maciaczyk J, Nikkhah G, et al. DiSCoVERing innovative therapies for rare tumors: combining genetically accurate disease models with *in silico* analysis to identify novel therapeutic targets. Clin Cancer Res 2016;22:3903–14.
33. Álvarez-Fernández M, Malumbres M. Mechanisms of sensitivity and resistance to CDK4/6 inhibition. Cancer Cell 2020;37:514–29.
34. Mertz JA, Conery AR, Bryant BM, Sandy P, Balasubramanian S, Mele DA, et al. Targeting MYC dependence in cancer by inhibiting BET bromodomains. Proc Natl Acad Sci U S A 2011;108:16669–74.
35. Bolin S, Borgenvik A, Persson CU, Sundstrom A, Qi J, Bradner JE, et al. Combined BET bromodomain and CDK2 inhibition in MYC-driven medulloblastoma. Oncogene 2018;37:2850–62.
36. Tang Y, Gholamin S, Schubert S, Willardson MI, Lee A, Bandopadhayay P, et al. Epigenetic targeting of Hedgehog pathway transcriptional output through BET bromodomain inhibition. Nat Med 2014;20:732–40.
37. Liang D, Yu Y, Ma Z. Novel strategies targeting bromodomain-containing protein 4 (BRD4) for cancer drug discovery. Eur J Med Chem 2020;200: 112426.
38. Rankovic Z, Min J, Mayasundari A, Keramatnia F, Jonchere B, Yang SW, et al. Phenyl-glutarimides: alternative cereblon binders for the design of PROTACs. Angew Chem Int Ed Engl 2021; 60:26663–70.
39. Singh MB, Sartor GC. BET bromodomains as novel epigenetic targets for brain health and disease. Neuropharmacology 2020;181:108306.
40. Henssen A, Thor T, Odersky A, Heukamp L, El-Hindy N, Beckers A, et al. BET bromodomain protein inhibition is a therapeutic option for medulloblastoma. Oncotarget 2013;4:2080–95.
41. Tarrado-Castellarnau M, de Atauri P, Tarrago-Celada J, Perarnau J, Yuneva M, Thomson TM, et al. De novo MYC addiction as an adaptive response of cancer cells to CDK4/6 inhibition. Mol Syst Biol 2017;13:940.
42. Freeman-Cook K, Hoffman RL, Miller N, Almaden J, Chionis J, Zhang Q, et al. Expanding control of the tumor cell cycle with a CDK2/4/6 inhibitor. Cancer Cell 2021;39:1404–21.
43. Liao S, Maertens O, Cichowski K, Elledge SJ. Genetic modifiers of the BRD4-NUT dependency of NUT midline carcinoma uncovers a synergism between BETis and CDK4/6is. Genes Dev 2018;32:1188–200.
44. Ge JY, Shu S, Kwon M, Jovanovic B, Murphy K, Gulvady A, et al. Acquired resistance to combined BET and CDK4/6 inhibition in triple-negative breast cancer. Nat Commun 2020;11:2350.
45. O'Brien NA, McDermott MSJ, Conklin D, Luo T, Ayala R, Salgar S, et al. Targeting activated PI3K/mTOR signaling overcomes acquired resistance to CDK4/6-based therapies in preclinical models of hormone receptor–positive breast cancer. Breast Cancer Res 2020;22:89.
46. Park AK, Lee JY, Cheong H, Ramaswamy V, Park SH, Kool M, et al. Subgroup-specific prognostic signaling and metabolic pathways in pediatric medulloblastoma. BMC Cancer 2019;19:571.
47. Skowron P, Farooq H, Cavalli FMG, Morrissy AS, Ly M, Hendrikse LD, et al. The transcriptional landscape of Shh medulloblastoma. Nat Commun 2021;12:1749.
48. Teo ZL, Versaci S, Dushyanthen S, Caramia F, Savas P, Mintoff CP, et al. Combined CDK4/6 and PI3Kα inhibition is synergistic and immunogenic in triple-negative breast cancer. Cancer Res 2017;77:6340–52.
49. Zhang Y, Yan H, Xu Z, Yang B, Luo P, He Q. Molecular basis for class side effects associated with PI3K/AKT/mTOR pathway inhibitors. Expert Opin Drug Metab Toxicol 2019;15:767–74.
50. Moreira DC, Venkataraman S, Subramanian A, Desisto J, Balakrishnan I, Prince E, et al. Targeting MYC-driven replication stress in medulloblastoma with AZD1775 and gemcitabine. J Neurooncol 2020;147:531–45.
51. Morfouace M, Nimmervoll B, Boulos N, Patel YT, Shelat A, Freeman BB III, et al. Preclinical studies of 5-fluoro-2'-deoxycytidine and tetrahydrouridine in pediatric brain tumors. J Neurooncol 2016;126:225–34.
52. Curran T. Reproducibility of academic preclinical translational research: lessons from the development of Hedgehog pathway inhibitors to treat cancer. Open Biol 2018;8:180098.
53. Ocasio J, Babcock B, Malawsky D, Weir SJ, Loo L, Simon JM, et al. scRNA-seq in medulloblastoma shows cellular heterogeneity and lineage expansion support resistance to SHH inhibitor therapy. Nat Commun 2019;10:5829.